EUROGRAPHICS 2025 / A. Bousseau and A. Dai
(Guest Editors)

COMPUTER GRAPHICS *forum*
Volume 44 (2025), Number 2

From Words to Wood: Text-to-Procedurally Generated Wood Materials

Mohcen Hafidi, Alexander Wilkie

Charles University

Figure 1: *A showcase of materials obtained from user interactions with our model, together with their corresponding textual inputs for the two levels of user experience we cater for. As with real wooden objects, various applications of the resulting 3D texture are possible: the objects on the table are machined from solid wood blocks, while the table itself is assumed to have been created via a process of bending wood over steam, so that the wood grain runs parallel to the curved surface. The > symbol is used to indicate separate text inputs from the user.*

Abstract

In the domain of wood modeling, we present a new complex appearance model, coupled with a user-friendly NLP-based front-end for intuitive interactivity. ***First****, we present a* ***procedurally generated wood model*** *that is capable of accurately simulating intricate wood characteristics, including growth rings, vessels/pores, rays, knots, and figure. Furthermore, newly developed features were introduced, including brushiness distortion, influence points, and individual feature control. These novel enhancements facilitate a more precise matching between procedurally generated wood and ground truth images.* ***Second****, we present a* ***text-based user interface*** *that relies on a trained natural language processing model that is designed to map user plain English requests into the parameter space of our procedurally generated wood model. This significantly reduces the complexity of the authoring process, thereby enabling any user, regardless of their level of woodworking expertise or familiarity with procedurally generated materials, to utilize it to its fullest potential.*

Keywords: procedural generation of wood, natural language processing, appearance modelling.

CCS Concepts
• **Computing methodologies** → **Volumetric models; Texturing;** *Information extraction;*

1. Introduction

This work addresses the task of realistically reproducing wood in computer graphics. The objectives of our work are twofold: **first**, we introduce a novel **Procedurally Generated Wood Model (PGWM)** that integrates State-Of-The-Art (SOTA) techniques into a unified framework. Our model also introduces new wood features and accommodates a wider variety of wood types within a single parameter space. **Second**, we make this PGWM instantly accessible across various user expertise levels via a Text-based User Interface (TUI).

Building on existing previous wood modelling efforts, the first part of our research mainly attempts to broaden the scope of the wood appearance features. Specifically, appearance features such as growth rings, pores, rays, figure, and knots. While the previously published papers on the topic established a solid foundation for realistic wood rendering, none of them encompass the complete array of appearance features simultaneously. We address these gaps by developing our PGWM, which not only handles existing wood features but also presents new ones to achieve a higher degree of photo-realism. As the resulting model is powerful but unwieldy, a critical innovation in our approach is the development of a TUI that is tightly coupled to the underlying PGWM. This interface is designed to simplify the modeling process, making it accessible and effortless for a broad range of users, from novices to experts.

In this investigation, we articulate several contributions to the domain of Procedural generation of wood materials. **Contribution 1** encompasses the development of a PGWM that integrates the nuanced visual characteristics of wood, advancing beyond the current SOTA. **Contribution 2** introduces an innovative TUI that revolutionizes the accessibility and ease of solid wood texture creation, enabling both novices and experts to generate photo-realistic materials with ease using the natural language they already know. In conjunction with our textual interface, we have developed a dataset of wood species predefined configurations designed to enhance the usability for novice users. This framework allows for the precise generation of well-known wood species using simple, direct commands, such as 'load pine wood >Add one knot >Change wood color to dark brown'.

The remainder of the paper is structured as follows: in Section 2, we discuss previous work in procedural wood modeling, and contrast existing techniques with the needs addressed by our current study. Section 3, Wood Identification, gives an in-depth overview of all the appearance features relevant to our PGWM. Following this, Section 4, Methodology, describes the technical execution of our PGWM and the innovative text-to-wood interface. In Section 5, Results, we present empirical evidence demonstrating the efficacy and advancements of our model over current methods. Section 6, Discussion, interprets the results, discussing implications, potential applications, and limitations of our work. Finally, Section 7, Conclusion, summarizes the key findings and proposes directions for future research.

2. Related Work

Procedural generation of wood materials. Generating wood textures, particularly through procedural generation for the wood grain, has been a focus of research since a long time in computer graphics. Notable contributions from [Pea85], [Lew89], and [LP00] have helped create patterns resembling natural growth rings and surface irregularities. However, the level of realism achieved remains relatively low.

In their work, Marschner et al. developed a shading model using BRDF (Bidirectional Reflectance Distribution Function) measurements to capture light scattering from subsurface wood fibers [MWAM05].

In their studies on the procedural generation of wood materials, Liu et al. explored the detailed features of wood, including fibers, vessels, growth rings, rays, and figures. Despite the depth of their research, their model, as discussed in [LMD15] and [LDHM16], did not incorporate knots and was complex in terms of parameter adjustments.

Larsson et al. [LIY*22] presented a procedural method for modeling wood with knots by applying a smooth minimum approach between distance fields. However, their approach did not extend to elements such as rays, figure, vessels, or knot cracks. Furthermore, the integration of growth rings with knots was not fully controllable, as the smooth minimum method relies on a single parameter to merge tree and knot distance fields.

The studies by Liu et al. [LDHM16], and Larsson et al. [LIY*22] relied on intensive tests to find values for the input parameters of the PGWM, making it extremely difficult for beginners without wood knowledge to utilize the model for a specific wood species. Inaccuracies in specifying these wood parameters can lead to unrealistic wood variants that do not naturally occur in reality.

Nindel et al. [NHIW23] presented an automatic method for matching procedurally generated wood to ground truth images by detecting growth rings with curved Gabor filters and using a phase-based loss function to capture anatomically accurate deformations. In the same area of research, Larsson and Ijiri et al. [LIS*] proposed a method for inferring the internal structure of wood based on surface photographs.

Kratt et al. [KSG*15] developed a simulation of tree growth and bark cracking that utilizes advanced methods to adapt to changing shapes and surfaces. Their system facilitates realistic modeling of growth, surface cracking, and stress effects, all of which are user-controllable.

2D image generation using AI techniques. Zhang et al. [ZLX*24] proposed a method for generating high-quality PBR materials using geometry- and light-aware diffusion models. Bensadoun et al. [BKA*24] presented a meta-learning-based approach for efficient and consistent texture generation for 3D objects, with both contributing to advancements in texture generation.

Stable diffusion [RBL*22; PYG*23], along with text-to-image generation innovations such as DALL-E 3, Imagen, and Midjourney [BGJ*23; SCS*22; Mid22], signify remarkable advancements in the realm of AI-driven creation. These technologies epitomize the cutting edge in synthesizing visual content from textual descriptions. It is natural to consider the use of such generative AI techniques for the creation of 2D wood textures: and it would be expected that high quality images of wood can be delivered by

such methods. However, wood is intrinsically a 3D material: and the limitation of 2D generated textures is visible at the edges of any 3D mesh, where textures on two sides of the edge do not realistically match and align. This issue underscores the critical need for procedural volumetric generation to ensure seamless, realistic wood textures.

3D material generation using AI techniques. While the AI-based 2D image generation techniques described in the previous paragraph have reached very high levels of sophistication, there are so far no corresponding methods for the direct generation of 3D appearance models. All one can do is to apply 2D images generated with 2D techniques as textures, which obviously fails in cases like wood or marble where the surface texture needs to correlate with the inner structure of an object. There are some recent generative approaches that take an entire 3D shape into account when generating consistent sets of 2D decal textures [LHL*24], but these would still only indirectly take any internal structure of the target *material* into consideration. All "knowledge" about the internal structure of the underlying material comes from the training data set, which makes it unlikely that the resulting model would flawlessly and reliably reproduce wood grain across multiple faces of a 3D object. Even though the authors of this work did not test their approach for wooden materials, the expectation would be that it would only partially perform at best, as the focus of the technique is not primarily on generating consistent surface features for 3D structures that are internal to the shape being textured.

NLP. Natural language processing approaches [CW14] allow information extraction from unstructured text as well as natural interaction in writing or a conversation. These range from traditional syntax-based methods like keyword detection to statistical NLP, and machine learning based language models which aim to capture the semantics of the text. Recently, large language models based on Generative Pre-Training (GPT [RNSS*18]) became popular, achieving state-of-the-art results in various tasks [Ope23], but their size (parameters count) makes them prohibitive to run on generally available hardware. Various statistical and other models to execute necessary language processing are readily available, e.g. in the spaCy library [HMVB20], which we use to implement the text interface of our wood model.

3. WOOD IDENTIFICATION

In this section, we give a brief overview of all the features that are relevant for wood appearance in a procedurally generated model.

Growth rings. Growth rings are the most prominent and distinguishable feature: they are concentric circles of varying width visible in a transverse section of a tree trunk. Each ring represents a single year's worth of growth, and typically consists of two layers: the usually lighter, wider section is called earlywood and it is formed during the spring, and the darker, denser section is called latewood and it is produced in the summer and autumn. These rings not only indicate the age of the tree but also provide insights into the environmental conditions it experienced during its growth, such as climate variations and weather events as studied in the field of Dendrochronology.

Heartwood and sapwood. In the transverse plane, two distinct regions can be identified: the inner section, known as heartwood, which in most cases darker in color, and the outer section, termed sapwood, which usually exhibits a lighter hue [Pou20]. As trees mature, they invariably undergo a physiological transformation whereby the innermost layers of sapwood progressively convert into heartwood, a process essential for structural reinforcement and increased resistance to environmental stressors.

Vessels/Pores. In a transverse cut of a tree, *pores* manifest as small, dark, irregularly shaped circular openings, this appearance is the result from cutting *vessels* [Pou20]. The unique feature that distinguishes hardwood from softwood is the presence of these vessels [WM05]. Vessels vary in diameter usually (0.01–0.2 mm) [CT14], and their lengths can range from as short as 1 millimeter (mm) to more than 10 meters (m) [CT14]. Hardwood species are classified based on pore size and distribution within a growth ring into ring-porous, semi-ring porous, and diffuse-porous categories [Pou20] (see Table 1) .

Rays. Rays are linear structures within a tree that extend radially from the center of the tree(i.e. the pith) outwards towards the bark(i.e. the outer later of the tree), appearing as lines with a distinctive color. Rays can contribute to the wood's appearance, particularly in species like oak, where pronounced rays create a decorative pattern known as ray fleck. The visibility of rays varies depending on the species.

Knots. Knots emerge at the points where branches were at some point present in the living tree. "Dead knots" are remainders of a branch that is still attached to the tree but have stopped growing - and they are characterized by a dark outline. Live knots lack this darkened border, indicating that the branch was alive and integrated into the tree's growth when encased. Knots can vary widely in size and color, and they are essentially the condensed essence of the tree's primary structure.

Figure. The *figure* of wood (its appearance of wood as seen on a longitudinal surface) is primarily influenced by the grain's orientation and irregularities. Unique patterns such as curls, ripples, and swirls emerge from variations in the wood fibers and the way the grain weaves through the tree's growth. This natural artistry of the grain is what gives figured wood its distinctive, highly sought-after appearance, turning ordinary timber into a canvas of natural beauty.

4. Methodology

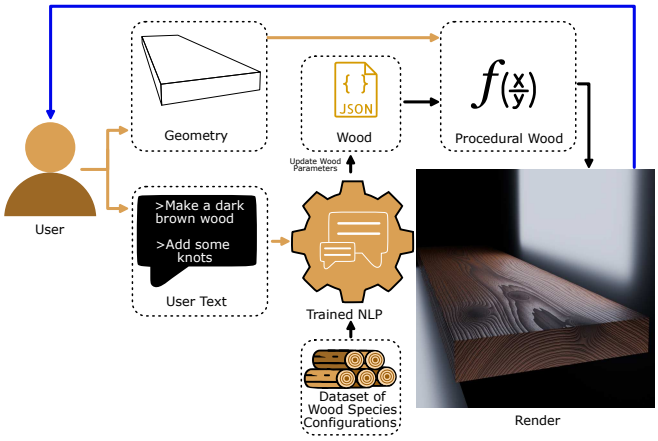

Figure 2: *Workflow in our proposed wood material authoring system.*

As shown in Figure 2, the process is initiated by the user input, which comprises both the 3D model's geometry and a textual description detailing the desired wood specie. This input is analyzed by the trained NLP model (Sec 4.2) that is designed to recognize the user's intentions and identify the requisite modifications to the wood parameters. To accommodate parameters not explicitly specified by the user, a dataset with predefined configurations for various wood species is employed. Subsequently, a JSON file containing all required parameters related to wood characteristics is updated and supplied to the PGWM (Sec 4.1), which renders the final visual output.

The generated results are then presented to the user, who may issue additional commands to further refine specific wood features within his current configuration. This iterative feedback loop continues until the user expresses satisfaction with the outcome. At this point, RGBA, roughness, and normal maps are generated, enabling the production of textures at any required resolution. These textures facilitate the creation of physically-based rendering (PBR) assets, applicable for both real-time and offline rendering usage.

4.1. Procedurally Generated Wood Model

In this section, we present our PGWM, where we detail the accurately modeled wood features alongside the textual experience. It is important to note that all mathematical operations and equations specified below are engineered to execute on a per-pixel basis within the framework of a GPU program.

4.1.1. Growth rings

The growth rings are modeled using a wave function, which mathematically describes the periodic oscillation of values representing the transitions between different regions in wood. We have tested several types of wave functions, such as: sine, square, triangle or sawtooth (see Figure 4). The wave function with the sawtooth comes closest to mimicking the ground-truth wood smooth transition from earlywood to latewood, and abrupt transition from one growth ring to another.

The main difference between our model for the growth rings and the one presented in [LDHM16] remains on the type of the wave function. The wave function used in [LDHM16] is a square wave function and ours is a sawtooth based function (see Figure 4).

To mathematically describe our sawtooth wave function to any given point $P(x,y,z)$ in the 3D space, we focus on the representation of the wave function, the masking for heartwood and sapwood, and the ease transition between earlywood and latewood.

1. Segment Lengths and Total Length Calculation
   Let $S = \{s_1, s_2, \ldots, s_n\}$ represent the set of segment lengths, where n is the total number of segments. The total length, L, of all segments is given by:
$$L = \sum_{i=1}^{n} s_i \tag{1}$$
2. Normalized Time Calculation
   The normalized time, T_{norm}, is calculated as:
$$T_{\text{norm}} = \text{mod}(Time \times TreeAge, L) \tag{2}$$
   Where $\text{mod}(a,b)$ denotes the modulus operation, returning the remainder of a divided by b. Here, $Time$ is the Euclidean distance (or magnitude) from the origin to the point $P(x,y,0)$, and $TreeAge$ is just a constant value.
3. Current Segment Identification
   The current segment index, k, is found where T_{norm} falls within the cumulative length up to that segment:
$$k = \min\left\{ k \mid \sum_{i=1}^{k} s_i > T_{\text{norm}} \right\} \tag{3}$$
4. Separating Heartwood and Pith from the other wood features:
   a. **Heartwood Mask M_{heart}**
   This mask is determined by comparing the normalized time, T_{norm}, against the cumulative lengths that represent the age of the heartwood. The assignment is as follows:
$$M_{\text{heart}} = \begin{cases} \text{Black} & \text{if } T_{\text{norm}} < \sum_{i=1}^{\text{heartwoodAge}} s_i \\ \text{White} & \text{otherwise} \end{cases} \tag{4}$$
   Black indicates areas within the heartwood age range, while white represents other parts of the wood.
   b. **Pith Mask M_{pith}**
   This mask is applied based on whether T_{norm} falls within the length of the first segment, identifying the pith region.
$$M_{\text{pith}} = \begin{cases} \text{Black} & \text{if } T_{\text{norm}} < s_1 \\ \text{White} & \text{otherwise} \end{cases} \tag{5}$$
   Here, black is used to highlight the pith, and white denotes areas outside the pith segment.
5. Sawtooth Wave Calculation Given the normalized time T_{norm}, segment lengths S, and an easing factor e, the smoothed wave

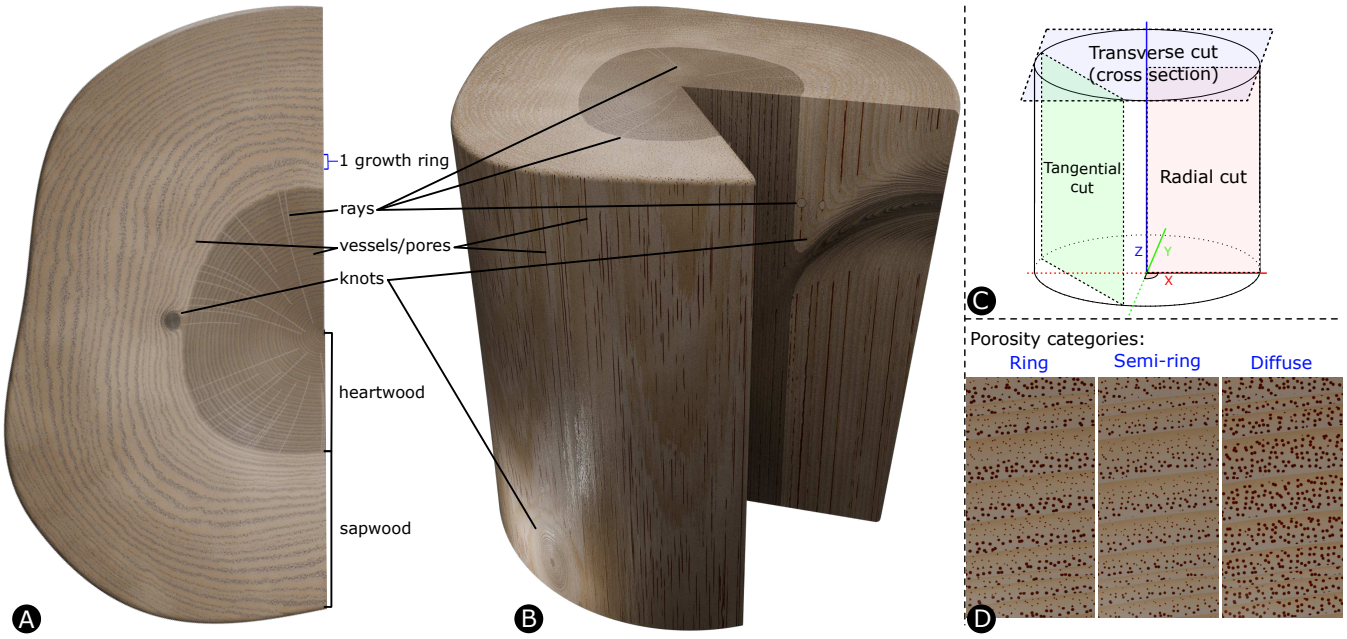

Figure 3: *Visualization of the wood features.(A) is a rendered image of a transverse section of the wood. (B) Is a rendered image of a tree trunk section, displaying wood properties from the two types of cuts transverse and radial.(C) is a diagram to show the different types of wood cuts in the wood working industries. (D) is a comparison between the different categories of porosity in a transverse cut. All the wood images are obtained using our PGWM.*

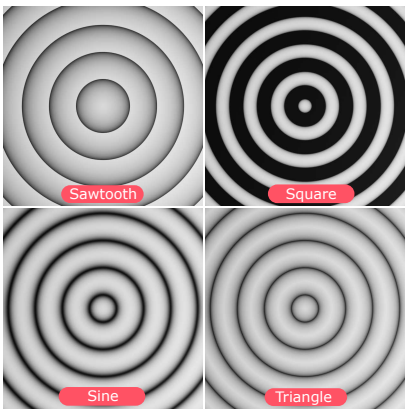

Figure 4: *Wave functions were compared using our wood model to simulate the growth rings visible in cross sections of wood. Our final model is based on the sawtooth wave function.*

value *Wave* within the current segment k is computed as follows:

$$Wave = \left(\frac{T_{\text{norm}} - \sum_{j=1}^{k-1} s_j}{s_k} \right)^e \tag{6}$$

This equation adjusts the wave's progression within each segment using the easing factor e, making it possible to adjust the transition from earlywood to latewood. The summation $\sum_{j=1}^{k-1} s_j$ calculates the cumulative length of all segments leading up to, but not including, the current segment k. This is a way of acknowledging how far along we are in the sequence of segments up to the point just before the current segment begins.

4.1.2. Vessels/Pores

We used Voronoi noise alongside our sawtooth wave function to model the vessels. We define a Piecewise Linear Function for each type of wood porosity (see Table 1), which controls the size of the pores. This approach allows us to accurately model the natural variability in pore sizes across different wood growth rings without overlapping the transition line between the latewood of the current growth ring and the earlywood of the next growth ring.

Our vessel model is comparable to the one described in [LDHM16]; however, our model exhibits greater precision control over the pores sizes through the application of the piecewise linear function, allowing for the avoidance of overlap with the extremities of growth rings (see Figure 3 (D)).

- For ring-porous types of wood: the pores' diameters have two states, large inside earlywood and small inside latewood. We model this variation using a 6-segment piecewise linear function that transitions between these states (see Table 1).
- For semi-ring porous types of wood: the diameter of the pores start large then gradually decreases from earlywood to latewood, the more we approach latewood the smaller the pores. We model this variation using a 4-segment piecewise linear function (see Table 1).
- For diffuse-porous types of wood: the diameter of the pores is

	Ring porous	Semi-ring porous	Diffuse porous
Segments' description	$\overline{P_0P_1}$: Pore size at growth ring boundaries is zero. $\overline{P_2,P_3}$: Small pore sizes in latewood. $\overline{P_4,P_5}$: Large pore sizes in earlywood. $\overline{P_1,P_2}$, $\overline{P_3,P_4}$, $\overline{P_5,P_6}$: Values during state transitions.	$\overline{P_0P_1}$: Pore size at growth ring boundaries is zero. $\overline{P_1,P_2}$: Gradually reducing pore size. $\overline{P_2,P_3}$: Values during state transitions. $\overline{P_3,P_4}$: Pore size at growth ring boundaries is zero.	$\overline{P_0P_1}$: Pore size at growth ring boundaries is zero. $\overline{P_2,P_3}$: large pores values for the whole growth ring. $\overline{P_1,P_2}$, $\overline{P_3,P_4}$: Values during state transitions.
Piecewise Linear Function	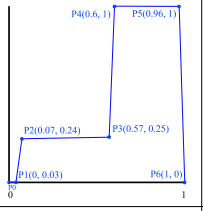	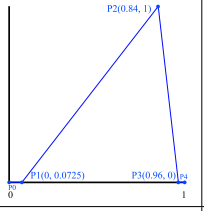	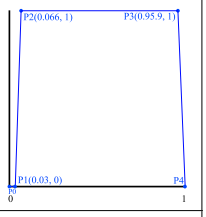
Rendered Diagrams of Pores	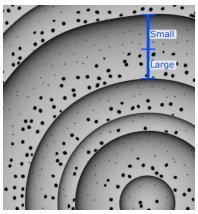	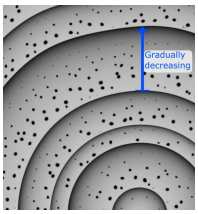	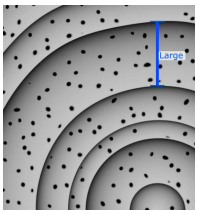
Microscopic structure [Bou08]	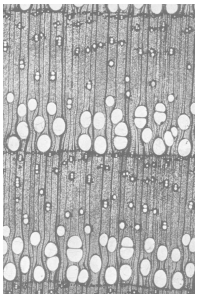 *Fraxinus americana*	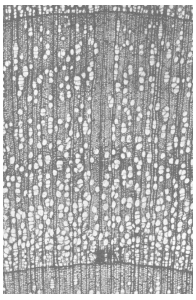 *Alnus glutinosa*	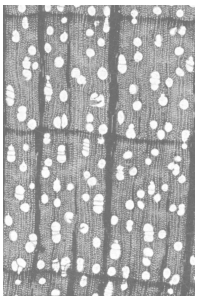 *Acer pseudoplatanus*

Table 1: *Comparative analysis of microscopic images [Bou08] of various pore distributions with rendered diagrams generated by our PGWM through the use of piecewise linear functions.*

generally the same and it is large, We model this using a 4-segment piecewise linear function (see Table 1).

In practice our model can shift from one porosity type to another or to not having pores at all using one parameter.

4.1.3. Rays

The previous state of the art wood model utilized the Wyvill kernel for rays modeling [LDHM16]. In our PGWM we decided to define a new rays model that is visually comparable to the one presented in [LDHM16]. Our model of rays is not visually worse or better than the previous SOTA model, we use different methods for the sake of simplification.

To mathematically describe our rays model, we will break it down into several parts:

Part 1: Defining an Elliptical Cylinder

In this part we define the function **f** that determines if any given point **p** in the 3D space is inside an elliptic cylinder. the resulting value of **f** is equal to 1 if **p** is inside and 0 else.

Variables and Parameters:

- p: input point in space, where $p = (x, y, z)$.
- s and e: Start and End points defining the cylinder's axis.
- h: cylinder height.
- b: the length of the semi-minor axis of the elliptic cylinder.
- a: the length of the semi-major axis of the elliptic cylinder.
- w: the vector $\overrightarrow{p_p p}$.
- r: the radial distance considering the length b.
- z: the distance from s to the projection of p onto $\overrightarrow{se}$.
- p_p: is the projection point of p into $\overrightarrow{se}$.

The elliptic cylinder indicator function f:

$$f(p,s,e,h,b,a) = \begin{cases} 1, & \text{if } 0 \le z \le h \text{ and } r < a \\ 0, & \text{otherwise} \end{cases} \tag{7}$$

where:

- $r = \sqrt{\mathbf{w}_x^2 + \mathbf{w}_y^2 + \left(\frac{\mathbf{w}_z}{b}\right)^2}$
- $p_p = s + z \cdot \overrightarrow{se}$
- $z = \overrightarrow{sp} \cdot \overrightarrow{se}$

Part 2: Defining Multiple Elliptical Cylinders Per Layer

Using the function **f**, we define the function **g**, which is responsible for defining multiple cylinders per layer. A single layer of cylinders simulates the rays from a cross-sectional slice of a tree, with each layer indexed by a specific z-coordinate value.

Variables and Parameters:

- n: total number of cylinders in each layer.
- s_z: the z coordinate of the starting point s of all the cylinders of the current layer.
- p_z: the point where $x = 0$, $y = 0$ and $z = s_z$.
- θ: the rotation value of the currant layer of cylinders.
- d_i: the random direction vector for the i-th cylinder.
- o_i: the offset random value for the i-th cylinder, used for shifting the cylinders from the pith of the tree to the outer bark.
- s_i and e_i: the start and end points that define the i-th cylinder's axis.

The layered cylinder aggregation function g:

$$g(p,n,s_z,h,b,a,\theta) = \sum_{i=1}^{n} f(p,s_i,e_i,h,b,a) \tag{8}$$

where:

- $s_i = p_z + d_i \cdot o_i$
- $e_i = s_i + d_i \cdot h$

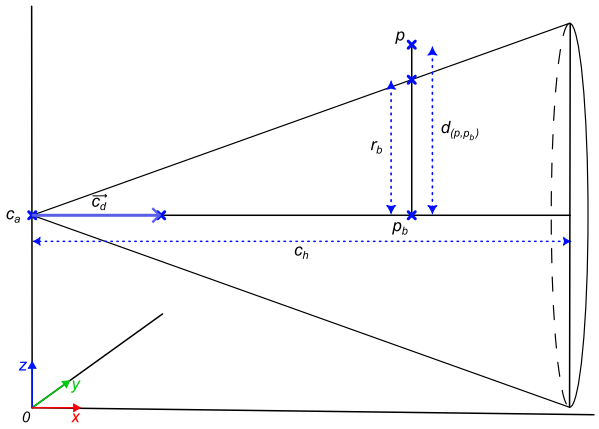

Figure 5: *Cone diagram, defining one knot before distortion.*

Part 3: Defining Multiple Layers of Elliptical Cylinders

We tried two methods to perform multiple layers of cylinders, the first one is to call the function g in a loop M times where the M is the number of layers, which was very expensive, the other method was to use the **Modulo** around the input Z coordinate and define the same layer of cylinders multiple times with a different rotation and distortion values, an offset value was used to define the spacing between layers to control the rays density around the Z axis.

4.1.4. Knots

In this section, we describe our model for simulating wood knots, with a particular focus on live knots. Our approach involves defining a cone system. Each cone represents a knot and is defined by its apex point and a direction vector. To define such a system for each point p in 3D space, we start by projecting the point p onto the axis of the current cone, which is defined by an apex c_a, a height c_h and a direction $\vec{c_d}$. This projection results in the point p_b. We then need to compute the distance $d(p, p_b)$ and the radius of the cone at the point p_b, which is r_b (see Figure 5). To determine if any given point p in the 3D space is inside the current cone, the conditions $d(p, p_b) \leq r_b$ and $0 \leq p_b < c_h$ need to be true. Note that this test is for one cone in the list of cones, a loop is required to test for all the cones in the cone system.

For the intersecting knots we use the smooth minimum function as mentioned in [LIY*22]. handling of the knots intersecting growth rings is described in section 4.1.8.

Up to this part of the paper we only described the knots as standard cones with no distortion. To achieve a closer shape to the ground-truth we apply a curvature function (c_f) to the radial distance (l_d), resulting in the curved value (c_v), this last one will then be used with the z value (p_z) of the input point p to compute the average value (a_v).

The input point of the resulting curved cone, defined as a geometric shape derived from a standard cone by applying a curvature function to the radial distances from its axis, is given by Equation 9.

$$\text{Curved\_Cone\_Point} = \mathit{Point}(p_x, p_y, a_v) \tag{9}$$

where:

- $l_d = \sqrt{p_x^2 + p_y^2}$
- $c_f(x) = \sqrt{1-(1-x)^2}$
- $c_v = c_f(l_d)$
- $a_v = \frac{p_z + c_v}{2}$

Our knots model does not cover all types of knots seen in [LIY*22] but presents an improved model for the live knots (see Figure 11). Some of the improvements, such as the random knots darkening are small improvements yet they significantly contribute to the visual realism side of the final result (see Figure 11). Another significant difference, and the reason we prefer to employ our knots model over the state-of-the-art (SOTA) knots model presented in [LIY*22], is that our model does not require any predefined data, such as the tree structure for determining knot location and orientation as shown in [LIY*22]. The absence of predefined tree data is essential to rendering it possible for users to interact with individual knots through the TUI.

4.1.5. Wood Distortion

One of the principal features that significantly enhances the realism of our wood model, absent from the SOTA models, is our innovative multi-distortion technique. This method is divided into two distinct parts: firstly, grain distortion, which is primarily visible at a macroscopic level and readily observable with the naked eye; and secondly, brushiness distortion, which becomes apparent at mesoscopic to microscopic scales. These techniques work in synergy to provide detailed wood distortion across the entire tree. We will discuss each of these parts in greater detail in the subsequent paragraphs.

Grain Distortion. The grain distortion is based on **influence points**, which exert a repulsive effect on the tree's growth rings, causing them to bend (see Figure 6). This approach is based on the repulsive and attractive forces principles, similar to those used in crowd simulations [TM12]. For flexibility in our model we allow for these influence points to be fully adjustable in terms of influence range, strength, position, and count.

Influence points. Influence points are specific control points within our PGWM, and can transition from random to manually defined distortions, for better matching between procedurally generated wood and a given ground truth. With this technique, we were able to closely match the wood photograph seen in Figure 9, a result not achieved in previous state-of-the-art work [LDHM16].

Brushiness distortion. Brushiness distortion is implemented using high-frequency nested Perlin noises elongated along the Z-axis. Due to the high frequency of noise, it induces subtle alterations in the growth rings, producing an effect akin to painting with a dry brush, hence the term 'brushiness distortion'.

In practice, the Z coordinate of P is divided by a high value (e.g., ten times its original value) for elongation. P is then sent as an input

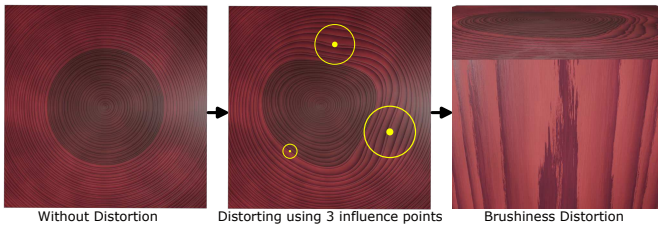

Figure 6: *Rendered results showing sequential stages of the distortion process depicted from left to right: initially, the undistorted tree; followed by grain distortion utilizing three* ***influence points*** *marked with yellow; and concluding with* ***brushiness distortion****.*

to a Perlin noise function, and the output, which is a scalar value from 0 to 1, is later used in another Perlin noise function. The exact parameters of the noise functions can vary depending on the type of wood.

Figure 6 depicts the progressive stages of the distortion process. All distortions are applied to the three-dimensional input point P before computing the wave function, as detailed in Section 4.1.1.

4.1.6. Normals

One of the most important outputs from our feature calculations on wood from the previous sections is the distance values, which range from 0 to 1. These values can be interpreted as height data. We can utilize this data to derive our normals, which will subsequently be used in our rendering process (see Figure 7).

Let $H(x,y)$ represent the height at any point (x,y) on a 3D texture surface. Here, the values of H are normalized between 0 and 1, where 0 represents the lowest elevation and 1 the highest.

Calculating Partial Derivatives. The process of converting height data into normal data in 3D requires calculating the partial derivatives of the height function H with respect to both x and y. These derivatives represent the slope of the surface at each point and are crucial for determining how the height variations contribute to the normal vector at each point:

$$H_x = \frac{\partial H}{\partial x} \tag{10}$$

$$H_y = \frac{\partial H}{\partial y} \tag{11}$$

Constructing the Normal Vector. In general the normal vector $\mathbf{N}$ at any point on a surface, is perpendicular to that surface. For a surface defined by a height map, the normal vector is influenced by the gradients H_x and H_y. The new modified normal vector at each point can be computed by:

$$\mathbf{N}_{\text{new}} = N + (-H_x, -H_y, 1) \tag{12}$$

$\mathbf{N}_{\text{new}}$ is then normalized to ensure it remains a unit vector. A visualization of the normal computation is shown in Figure 7

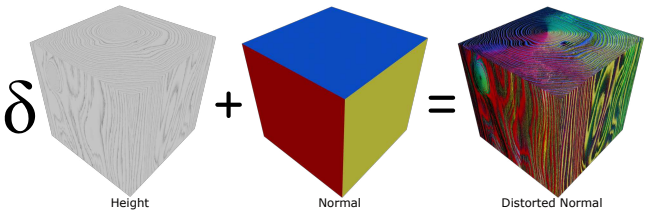

Figure 7: *Visualization of distorted normals computation.*

4.1.7. Roughness

Earlywood tends to have higher roughness and is less shiny due to its more absorbent nature, while latewood exhibits lower roughness and appears shinier as it is less absorbent [GUR14]. Similarly to the normal computation we compute the roughness from the distance values, and map the distance values from the range of 0 to 1 to the range of 0.3 to 0.7, these values are the average values obtained from multiple studies about roughness in earlywood and latewood [PKPS16] [ZHC13] [Dav11] of several wood species, these values are used as default for the unknown roughness values in our wood dataset configurations.

4.1.8. Merging all the wood features

Until now we explained how we modeled the wood features separately, but an additional challenging aspect of procedural generation of materials is merging all these features into a single, integrated model.

Growth rings and knots. To merge growth rings and wood knots a smooth minimum function could be used (see [LIY*22]). We drooped the use of the smooth minimum technique, and opted for a three-point Bézier curve to prepare the knot for merging with the distorted main radial distance of the tree. This same Bézier curve is utilized to control the knot's age without affecting the tree grain (see Figure 8).

The used Bézier curve is defined by three points $P_1(0.0, 0.356)$, $P_2(0.283, 0.913)$, and $P_3(1.0, 0.955)$ and is given by:

$$B(t) = (1-t)^2 P_1 + 2(1-t)tP_2 + t^2 P_3, \quad t \in [0,1] \tag{13}$$

Expanding this, we have:

$$B(t) = \left(0.566(1-t)t + t^2,\ 0.356(1-t)^2 + 1.826(1-t)t + 0.955t^2\right) \tag{14}$$

t is the parameter that defines the current position along the curve, in our case it is the radial distance of the curved cone seen in 4.1.4.

A simple multiplication is later performed between the scalar value obtained from the equation 14 and the radial distance obtained from the distorted main tree to compute the distance field. This latter one will then be used as an input for the sawtooth wave computation seen in section 4.1.1.

Growth rings and vessels. The wave value given by Equation 6 is used as an input value to the Piecewise Linear Functions used in 4.1.2, this way we indicate where earlywood and latewood are, and where the transitions in-between them are placed.

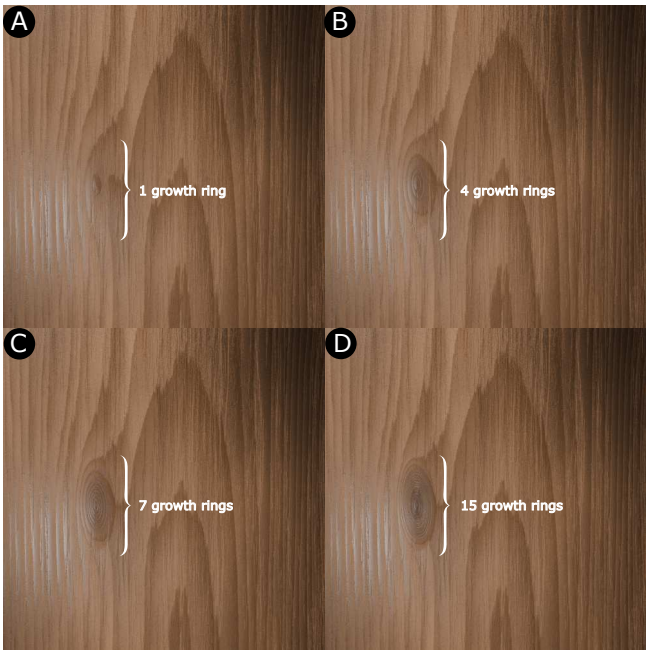

Figure 8: *From A to D, resp. we are decreasing the coordinate Y value of the point P2 from the Bézier curve defined in 4.1.8. In this figure we show the exceptional ability of controlling the knot age without affecting the main tree grain.*

Rays and other wood features. Wood rays overlap the growth rings and the vessels, so we used the distance value of the rays to mask them off the growth rings, and off the vessels.

4.1.9. Dataset of wood species configurations

To ensure the flexibility of our model in handling inputs not explicitly provided by users, we have developed a dataset comprising predefined configurations for various wood species. This dataset is contained within a single JSON file, which encompasses multiple entries for different wood species. Each entry is structured as a dictionary representing a specific wood species, encapsulated with a set of parameters and their corresponding predefined values.

The derivation of these values is based on individual evaluations. We have precisely defined certain parameters, such as the type of porosity, which may be categorized as ring-porous, semi-ring-porous, or diffuse; and the level of roughness, which has been previously studied and quantified by other researchers. However, due to resource limitations, some parameters were approximated in a less rigorous manner. Examples of these include the manual color selection for earlywood, latewood, sapwood, and heartwood from photographic sources, and the estimation of ray density.

While some parameters values are approximated some others are constructed from scientific papers and trusted resources [Ab], [GUR14], [Mei15], and [Enc23].

It is important to note that this dataset includes only parameters and their corresponding values, and does not contain any images.

4.2. Text to Wood

A significant limitation of existing PGWMs (Procedurally Generated Wood Models), such as those developed by [LDHM16] and [LIY*22], is their complex user interfaces. The vast diversity of wood species and their characteristics necessitate numerous parameters to configure the model for a certain wood species. This complexity can pose significant challenges for users without extensive expertise in wood characteristics and, perhaps even more so, working with complex multi-parameter procedurally generated models. To address this, we introduce a user-friendly text interface to our PGWM, enabling users of all skill levels to easily modify parameters using natural language, thus removing the need for specialized technical knowledge.

NLP enables computers to understand human language, one of its practical applications is entity recognition which is what we employed to build our text to PGWM.

Our approach utilizes Named Entity Recognition (NER) to identify and categorize key information in the text — specifically, terms related to various wood properties. To develop our custom NER model, we began by assembling a targeted dataset consisting of 500 lines of wood descriptions. This dataset includes phrases typical of procedural generation of wood, such as ‘take off the knots‘, ‘raise the vessels’ scale by 12%‘, and ‘change the colour intensity of the vessels to light red.‘ Each phrase was annotated to mark the start and end indices of each entity and its type, a critical step for ensuring the training accuracy of our model.

To elucidate the annotation process used in our Named Entity Recognition (NER) model, consider the specific example of the phrase ‘Raise the vessels’ scale by 12%’. This sentence illustrates how natural language instructions are systematically broken down and categorized to facilitate the model’s understanding and processing capabilities.

- **‘raise’**: Labeled as ***Increase***, indicating the operation to be performed.
- **‘the vessels scale’**: Labeled as ***Vessels_scale***, specifying the wood parameter to be edited.
- **‘12%’**: Labeled as ***Percentage***, quantifying the change to be made to ***Vessels_scale***.

Each component of the sentence is tagged with its respective role in the command, allowing the model to parse and execute changes based on user inputs efficiently.

The result from the labeling process is obtained in the following format:

```
("raise␣the␣vessels'␣scale␣by␣12%", {"
    entities": [(0, 5, "Increase"), (6, 23,
    "Vessels_scale"), (27, 30, "Percentage")
    ]})
```

In order to employ this with spaCy, the format will be transformed into a structure that spaCy can interpret:

```
"classes": [
    "INCREASE", "VESSELS_SCALE", "PERCENTAGE
        "
```

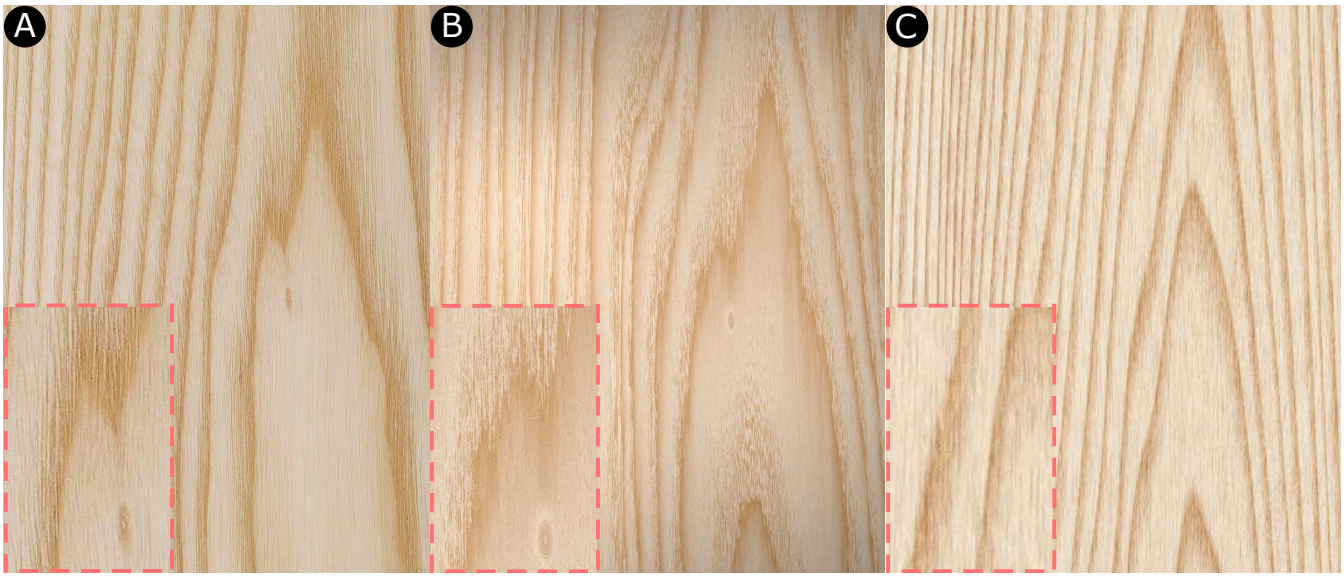

Figure 9: *Ash wood. Our result (B) is compared to the ground truth (A) and the results from the SOTA paper [LDHM16] (C). The wood model in [LDHM16] depends solely on randomness to distort the wood grain and does not match the ground-truth (A). Our approach on the other hand utilizes influence points to precisely model annual rings, we were also able to simulate the tiny knot observed in (A).*

```
],
"annotations":
    ["raise␣the␣vessels'␣scale␣by␣12%.",
        {
            "entities": [
                [
                    0,5,"INCREASE"
                ],[
                    10,24,"␣VESSELS_SCALE"
                ],[
                    28,31,"PERCENTAGE"
    ]]}]
```

This structured tagging is critical for enabling the model to interpret user commands accurately and for adjusting the model parameters accordingly.

Now that the training dataset was prepared, we utilized the comprehensive en_core_web_lg model from spaCy, focusing specifically on its NER component, as the foundational layer for our custom model. Starting with this pre-trained base, we initialized a spaCy model, which we tailored to our specific needs. After only 51 minutes of one training cycle with our carefully annotated dataset, we fine-tuned the model to accurately recognize and categorize the set of wood-specific parameters, user intents, and the types of values needed for parameter update. This significantly enhanced the model's understanding of wood terminology within textual inputs. As a result, we now have a trained model capable of precisely recognizing user inputs.

The bridge between the outputs of our NLP model and the final updated JSON file is managed by a Python script set up as a hierarchy of conditional statements. This script receives predefined commands (e.g., 'increase', 'decrease', or 'set') alongside wood-specific parameters (e.g., 'wood-age' or 'earlywood-color') and values (e.g., '12%', '255,0,0', or '155.40'). It systematically navigates these inputs through conditional branching to dictate specific modifications to a wood parameter within the JSON file, ensuring each command is accurately translated from text to a parameter update. Consequently, this process effects real-time and precise updates to the wood model parameters. In instances where critical components such as the intent, parameter name, or value are missing (i.e. not recognized by the NLP model), the script defaults to a failure mode, as illustrated in Figure 10.

5. Results

In Figure 1 and 10 we demonstrate how a novice and an expert user would work with our system to model a particular wood species. This showcases the capabilities of our PGWM and how easy our text interface makes it to achieve complex and interesting materials. With our system, users do not need to be experts in wood or in procedural generation to achieve realistic results. At the same time, procedural material generation experts can also make detailed changes to all components.

In a system like Blender, the mathematical functions of our PGWM could be implemented through Open Shading Language (OSL) shaders, which are commonly referred to as custom nodes in the shader editor. Each node can be defined with specific inputs and outputs, forming a directed acyclic graph. This graph's outputs are parameter values that serve as inputs to functions such as the Spatially-Varying Bidirectional Scattering Distribution Function (SVBSDF).

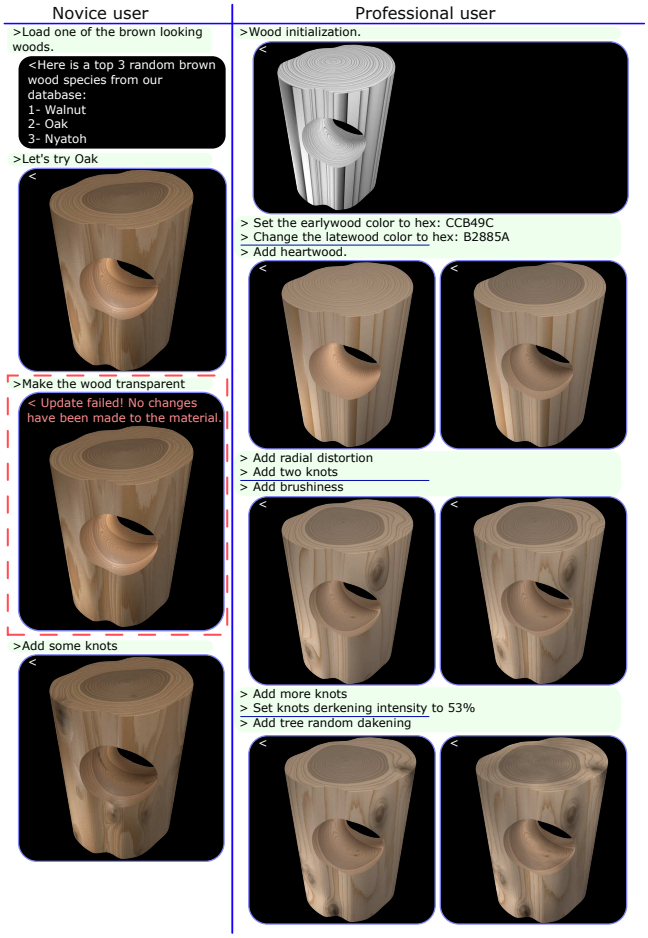

Figure 10: *Example sessions of two users at different skill levels. Note that our model is capable of interpreting both vague and specific commands, and that expert users can make very specific demands with regard to colors and other model parameters. The case highlighted with a dashed red border is the standard reply of our system to failure cases where the system can not make sense of a user input.*

Comparison with prior work. In Figure 11 we show a comparison study between our wood model and the most recent PGWM that features knots by [LIY*22]. We used the authors' implementation to get the results in Figure 11 (C). The prominent differences between the SOTA model and ours in this figure are: 1) The non uniform darkening of the knots, in reality knots are not uniformly darker than the main tree. 2) If we zoom into the ground-truth image we can see the heartwood (i.e. the darker area that is in the center of the knot). 3) Other wood features, such as roughness and brushiness distortion, can create significant visual differences between the two models.

Figure 3 showcases the majority of wood features implemented in our PGWM, with a particular emphasis on the interaction between key elements such as rays, vessels, growth rings, and knots.

The comparison with the PGWMs by [LDHM16] and [LIY*22]

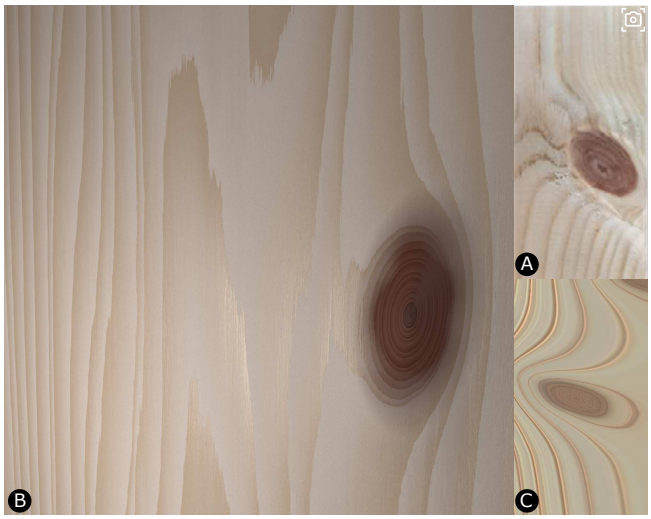

Figure 11: *Our knot B) compared to ground-truth A) and to results obtained from utilizing the GitHub repository project provided by [LIY*22] C)*

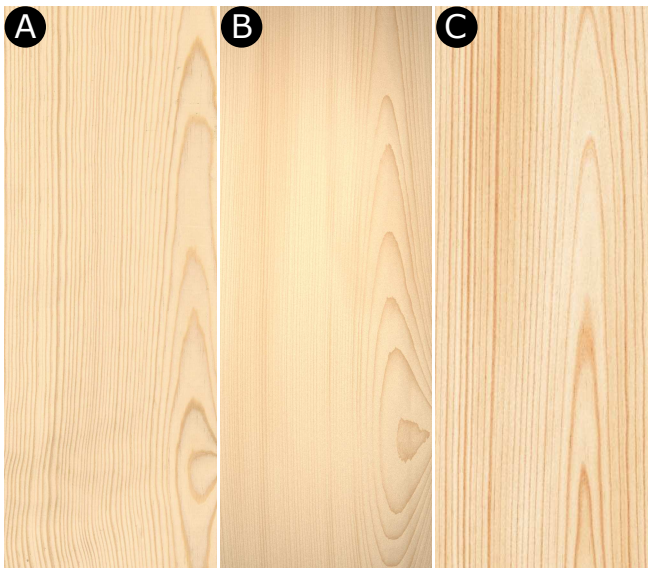

Figure 12: *Pine wood. Our result (B) is compared to the ground truth (A) and to the results from the SOTA paper [LDHM16] (C). The pinching effect on the bottom right corner observed in (A) is likely caused by a wood knot, and could be replicated with our model by placing a knot at that exact location, which can not be the case for (C) since the knot feature is not implemented.*

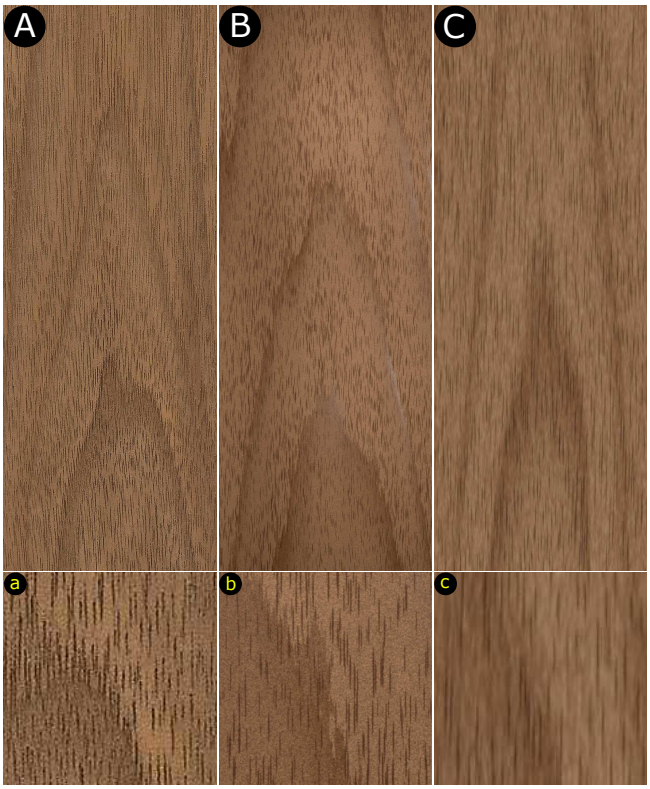

Figure 13: *Walnut wood. Our result (B) is compared to the ground truth (A) and to the results from the SOTA paper [LDHM16] (C).*

highlights significant improvements, such as the brushiness distortion that shows a noticeable visual improvement (see Figures 9, 12, and 13), the capability of individually editing a wood feature, the heartwood and sapwood, and the influence points for a more precise distortion of the wood grain. All these improvements are clearly accurately reflecting the natural wood characteristics.

Figure 9 specifically illustrates the ability of our PGWM to precisely distort the wood grain, a feature that is absent in the PGWM by [LDHM16]. This precision was achieved through the use of influence points, which allow for accurate shaping of the annual rings. Additionally, our model successfully simulated the current knot in the ground-truth image, a feature that is not supported by [LDHM16].

The wood figure feature is a unique characteristic of the model proposed by [LDHM16]. Despite the complexity of the spiral techniques employed in the SOTA model, we successfully replicated the results using height maps as an alternative approach. The computations detailed in Section 4.1.6 were applied to convert height maps into normal maps. The rendered results are shown in Figure 14.

The table 2 compares features of PGWMs, highlighting key distinctions between our model and those developed by [LDHM16] and [LIY*22]. It is important to note that some features are not implemented across all three models, leaving opportunities for future research.

	Ours	**Larsson et al.**	**Liu et al.**
Growth rings	✓	✓	✓
Vessels or Pores	✓	X	✓
Rays	✓	X	✓
Live knots	✓	✓	X
Dead knots	X	✓	X
Ended knots (broken branches)	X	X	X
Random tree distortion	✓	X	✓
Custom grain distortion	✓	X	X
Vessels shape distortion	✓	X	X
Non-uniform Knots darkening	✓	X	X
Early-to-latewood ease control	✓	X	✓
Per growth ring size and ease control	✓	X	X
Brushiness Distortion	✓	X	X
Normal/Bump	✓	X	✓
Roughness	✓	X	✓
Random Tree Darkening	✓	X	✓
Heartwood and Sapwood	✓	Color mapped	X
Wave function	Sawtooth	Color mapped	Square
Figure	Using a height map	X	✓
Wood Cracks	X	X	X
Inner and Outer barks	X	X	X
Requirements for using the Model	None, thanks to the TUI, everything can be edited using plain English	procedural generation, and wood knowledge needed	procedural generation, and wood knowledge needed
Performance of the PGWM	1 frame per text instruction, but real-time using PBR textures	real-time	real-time

Table 2: *Comparison table of prior PGWMs, showing key differences between our model, Liu et al. [LDHM16], and Larsson et al. [LIY*22].*

6. Discussion

In their research, Lee et al. [LY16] explored the advantages of text-based interfaces compared to traditional graphical user interfaces (GUIs) across various scenarios. They specifically highlight the effectiveness of text-based commands in dimensionality reduction, such as scripting animations, which bears a strong resemblance to our method of tuning parameter values for the PGWM. Building on the insights from Lee et al., and complemented by the 14 cases of a non-formal user study conducted by our internal team, depicted in Figures 1 and 10, we assert that the text-based interface enhances the efficiency of interacting with the PGWM for both novice and expert users. Moreover, we acknowledge that the lack of a more comprehensive user study performed with our system is a limitation of our current research, and requires future investigation.

Regarding the robustness of our system, as illustrated in Fig. 10, the system retains its state between queries, and so allows incremental modifications of the results based on user commands. For example, instructing the system to ‘change the age of the tree to 500’ from a previous age of 100 markedly increases the number of rings within the tree, representing a significant alteration. In contrast, a minor command such as ’Set knots darkening intensity to 53%’ from an initial 50% results in a change that is nearly indiscernible.

For real-time applications such as a tree-cutting simulator, the performance of our system is significantly influenced by the hardware due to its use of both CPU and GPU in its current implementation. However, if the requirement is to use a 3D mesh as an asset, it is feasible to bake textures from our PGWM. The resulting PBR

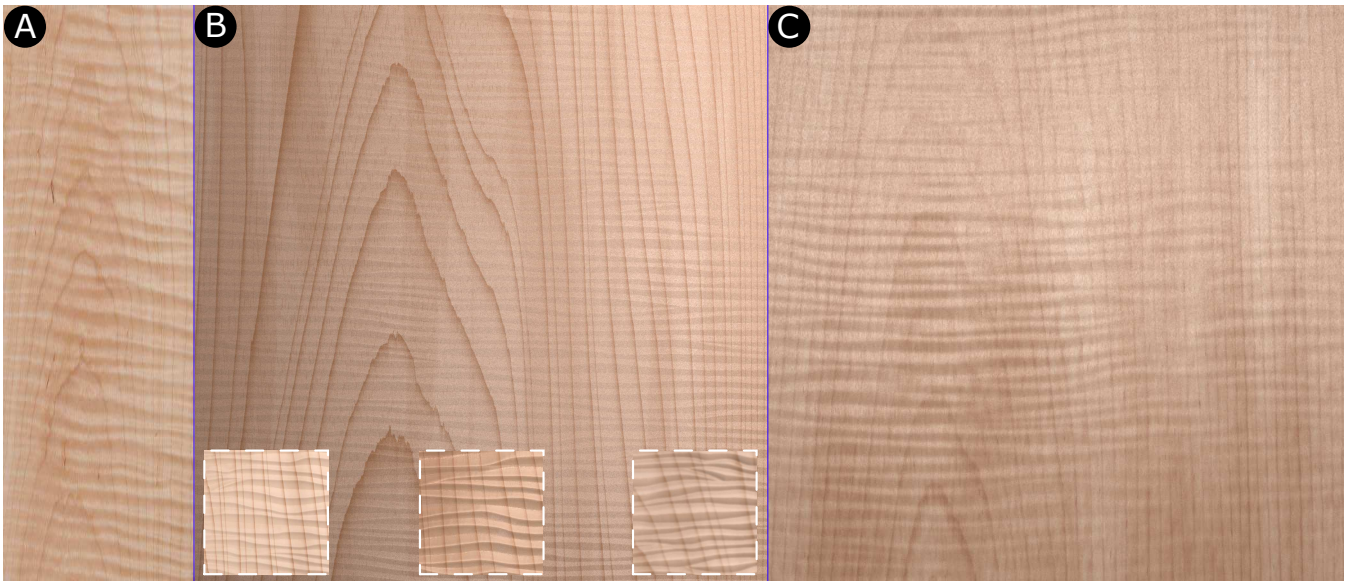

Figure 14: *The wood figure feature. Our results (B) are compared to the ground truth (A) and to the results from the SOTA paper [LDHM16] (C). We were able to replicate the results using one of the height maps presented in [LDHM16] and the calculations seen in 4.1.6. Variations in (B), highlighted within white squares, are achieved by adjusting the height map's strength and the light sources in our scene.*

textures can then be used in conjunction with the input mesh inside of a real-time environment. A full GPU implementation of our model could further enhance its efficiency and real-time capabilities.

The NLP interface and PGWM have notable limitations. The NLP struggles with undefined parameters and syntax errors, leading to the system ignoring commands. The PGWM currently does not account for wood treatments like staining or varnishing and also lacks features such as parenchyma or wood bark.

7. Conclusion

This study presents a significant advancement in procedural wood generation by enhancing the visual realism of 3D wood textures through detailed modeling of wood features such as growth rings, vessels, knots, rays, figure, and others. Our model leverages procedural techniques to achieve realism. Complementing this, we introduce a user-friendly, NLP-based interface model that allows straightforward manipulation of the wood complex features through textual commands. This dual approach not only improves the model's accessibility but also significantly reduces the technical barriers associated with procedural wood generation, broadening its appeal to a wider audience.

Despite these advancements, there are limitations in the current implementation. The NLP interface is sensitive to input errors and limited to existing parameters, requiring fine-tuning the model for expansions. The PGWM currently lacks wood features such as cracks and tree bark which are not yet modeled and left for future works.

Moving forward, efforts will focus on enhancing the NLP model's robustness, expanding the PGWM's capabilities to include missing features, and improving safeguards against unrealistic outputs. These improvements aim to extend the model's utility in various fields, making advanced wood modeling techniques more accessible and user-friendly for both novices and experts.

Acknowledgments. We express our sincere appreciation to Martin Mirbauer for his extensive support throughout the project and to Ali Ahmed Maher Dali for his expert assistance in data processing. This work received funding from the European Union's Horizon 2020 research and innovation program under the Marie Sklodowska-Curie grant agreement No 956585, and from the Czech Science Foundation (GAČR) grant No. 22-22875S, which we gratefully acknowledge. The work was supported by the grant SVV-2025-260822. Open access publishing facilitated by Univerzita Karlova, as part of the Wiley – CzechELib agreement.

References

[Ab] ANAGNOST, SUSAN and BENZINK. *Database of scanned wood at microscopic level*. URL: https://ncbrownultrastructure.wordpress.com/ 9.

[BGJ*23] BETKER, JAMES, GOH, GABRIEL, JING, LI, et al. "Improving image generation with better captions". (2023). URL: https://cdn.openai.com/papers/dall-e-3.pdf 2.

[BKA*24] BENSADOUN, RAPHAEL, KLEIMAN, YANIR, AZURI, IDAN, et al. "Meta 3D TextureGen: Fast and Consistent Texture Generation for 3D Objects". *arXiv preprint arXiv:2407.02430* (2024) 2.

[Bou08] BOULGER, GEORGE SIMONDS. *Wood: a manual of the natural history and industrial applications of the timbers of commerce*. E. Arnold, 1908 6.

[CT14] CAI, JING and TYREE, MELVIN T. "Measuring vessel length in vascular plants: can we divine the truth? History, theory, methods, and contrasting models". *Trees* 28.3 (June 2014), 643–655. ISSN: 1432-2285. DOI: 10.1007/s00468-014-0999-9. URL: https://doi.org/10.1007/s00468-014-0999-9 3.

[CW14] CAMBRIA, ERIK and WHITE, BEBO. "Jumping NLP Curves: A Review of Natural Language Processing Research [Review Article]". *IEEE Computational Intelligence Magazine* 9.2 (2014), 48–57. DOI: 10.1109/MCI.2014.2307227 3.

[Dav11] DAVIM, J. PAULO. "Evaluating the Roughness of Sanded Wood Surfaces". *Wood Machining*. John Wiley & Sons, Ltd, 2011. Chap. 6, 217–267. ISBN: 9781118602713. DOI: https://doi.org/10.1002/9781118602713.ch6. eprint: https://onlinelibrary.wiley.com/doi/pdf/10.1002/9781118602713.ch6. URL: https://onlinelibrary.wiley.com/doi/abs/10.1002/9781118602713.ch6 8.

[Enc23] ENCYCLOPAEDIA BRITANNICA. *Wood (plant tissue) - Microstructure*. Accessed: 2023-05-19. 2023. URL: https://www.britannica.com/science/wood-plant-tissue/Microstructure 9.

[GUR14] GURĂU, LIDIA. "The influence of earlywood and latewood upon the processing roughness parameters at sanding." *Pro Ligno* 10.3 (2014) 8, 9.

[HMVB20] HONNIBAL, MATTHEW, MONTANI, INES, VAN LANDEGHEM, SOFIE, and BOYD, ADRIANE. "spaCy: Industrial-strength Natural Language Processing in Python". (2020). DOI: 10.5281/zenodo.1212303 3.

[KSG*15] KRATT, J., SPICKER, M., GUAYAQUIL, A., et al. "Woodification: User-Controlled Cambial Growth Modeling". *Computer Graphics Forum* 34.2 (2015), 361–372. DOI: https://doi.org/10.1111/cgf.12566. eprint: https://onlinelibrary.wiley.com/doi/pdf/10.1111/cgf.12566. URL: https://onlinelibrary.wiley.com/doi/abs/10.1111/cgf.12566 2.

[LDHM16] LIU, ALBERT JULIUS, DONG, ZHAO, HAŠAN, MILOŠ, and MARSCHNER, STEVE. "Simulating the Structure and Texture of Solid Wood". *ACM Trans. Graph.* 35.6 (Dec. 2016). ISSN: 0730-0301. DOI: 10.1145/2980179.2980255. URL: https://doi.org/10.1145/2980179.2980255 2, 4–7, 9–13.

[Lew89] LEWIS, J.-P. "Algorithms for solid noise synthesis". *Proceedings of the 16th Annual Conference on Computer Graphics and Interactive Techniques (SIGGRAPH '89)*. 1989, 263–270 2.

[LHL*24] LE, CINDY, HETANG, CONGRUI, LIN, CHENDI, et al. *EucliDreamer: Fast and High-Quality Texturing for 3D Models with Stable Diffusion Depth*. 2024. arXiv: 2311.15573 [cs.CV] 3.

[LIS*] LARSSON, MARIA, IJIRI, TAKASHI, SHEN, I-CHAO, et al. "Learned Inference of Annual Ring Pattern of Solid Wood". *Computer Graphics Forum* n/a.n/a (), e15074. DOI: https://doi.org/10.1111/cgf.15074. eprint: https://onlinelibrary.wiley.com/doi/pdf/10.1111/cgf.15074. URL: https://onlinelibrary.wiley.com/doi/abs/10.1111/cgf.15074 2.

[LIY*22] LARSSON, MARIA, IJIRI, TAKASHI, YOSHIDA, HIRONORI, et al. "Procedural Texturing of Solid Wood with Knots". *ACM Trans. Graph.* 41.4 (July 2022). ISSN: 0730-0301. DOI: 10.1145/3528223.3530081. URL: https://doi.org/10.1145/3528223.3530081 2, 7–9, 11, 12.

[LMD15] LIU, ALBERT J., MARSCHNER, STEPHEN R., and DYE, VICTORIA E. *Procedural wood textures*. 2015. arXiv: 1511.04224 [cs.GR]. URL: https://arxiv.org/abs/1511.04224 2.

[LP00] LEFEBVRE, L. and POULIN, P. "Analysis and synthesis of structural textures". *Proceedings of Graphics Interface*. 2000, 77–86 2.

[LY16] LEE, SANGWON and YAN, JIN. "The Potential of a Text-Based Interface as a Design Medium: An Experiment in a Computer Animation Environment". *Interacting with Computers* 28.1 (2016), 85–101. DOI: 10.1093/iwc/iwu036 12.

[Mei15] MEIER, ERIC. *WOOD! Identifying and using hundreds of woods worldwide*. Wood Database, 2015. ISBN: 978-0-9822460-3-0 9.

[Mid22] MIDJOURNEY, INC. *Midjourney*. 2022. URL: https://www.midjourney.com/ 2.

[MWAM05] MARSCHNER, STEPHEN R., WESTIN, STEPHEN H., ARBREE, ADAM, and MOON, JONATHAN T. "Measuring and Modeling the Appearance of Finished Wood". *ACM SIGGRAPH 2005 Papers*. SIGGRAPH '05. Los Angeles, California: Association for Computing Machinery, 2005, 727–734. ISBN: 9781450378253. DOI: 10.1145/1186822.1073254. URL: https://doi.org/10.1145/1186822.1073254 2.

[NHIW23] NINDEL, THOMAS K., HAFIDI, MOHCEN, ISER, TOMÁŠ, and WILKIE, ALEXANDER. *Automatic inference of a anatomically meaningful solid wood texture from a single photograph*. 2023. arXiv: 2302.01820 [cs.GR]. URL: https://arxiv.org/abs/2302.01820 2.

[Ope23] OPENAI. *GPT-4 Technical Report*. 2023. arXiv: 2303.08774 [cs.CL] 3.

[Pea85] PEACHEY, D. R. "Solid texturing of complex surfaces". *Proceedings of the 12th Annual Conference on Computer Graphics and Interactive Techniques (SIGGRAPH '85)*. 1985, 279–286 2.

[PKPS16] PINKOWSKI, GRZEGORZ, KRAUSS, ANDRZEJ, PIERNIK, MAGDALENA, and SZYMAŃSKI, WALDEMAR. "Effect of thermal treatment on the surface roughness of scots pine (Pinus sylvestris L.) wood after plane milling". *BioResources* 11.2 (2016), 5181–5189 8.

[Pou20] POURNOU, ANASTASIA. *Biodeterioration of Wooden Cultural Heritage*. Springer Cham, 2020. ISBN: 978-3-030-46504-9. URL: https://doi.org/10.1007/978-3-030-46504-9 3.

[PYG*23] PO, RYAN, YIFAN, WANG, GOLYANIK, VLADISLAV, et al. *State of the Art on Diffusion Models for Visual Computing*. 2023. arXiv: 2310.07204 [cs.AI] 2.

[RBL*22] ROMBACH, ROBIN, BLATTMANN, ANDREAS, LORENZ, DOMINIK, et al. "High-Resolution Image Synthesis With Latent Diffusion Models". *Proceedings of the IEEE/CVF Conference on Computer Vision and Pattern Recognition (CVPR)*. June 2022, 10684–10695 2.

[RNSS*18] RADFORD, ALEC, NARASIMHAN, KARTHIK, SALIMANS, TIM, SUTSKEVER, ILYA, et al. "Improving language understanding by generative pre-training". (2018) 3.

[SCS*22] SAHARIA, CHITWAN, CHAN, WILLIAM, SAXENA, SAURABH, et al. "Photorealistic Text-to-Image Diffusion Models with Deep Language Understanding". *Advances in Neural Information Processing Systems*. Ed. by KOYEJO, S., MOHAMED, S., AGARWAL, A., et al. Vol. 35. Curran Associates, Inc., 2022, 36479–36494. URL: https://proceedings.neurips.cc/paper_files/paper/2022/file/ec795aeadae0b7d230fa35cbaf04c041-Paper-Conference.pdf 2.

[TM12] THALMANN, DANIEL and MUSSE, SORAIA RAUPP. *Crowd Simulation*. 2nd. Springer Publishing Company, Incorporated, 2012. ISBN: 144714449X 7.

[WM05] WIEDENHOEFT, ALEX C and MILLER, REGIS B. "Structure and function of wood". *Handbook of wood chemistry and wood composites* (2005) 3.

[ZHC13] ZHONG, Z.W., HIZIROGLU, SALIM, and CHAN, C.T.M. "Measurement of the surface roughness of wood based materials used in furniture manufacture". *Measurement* 46.4 (2013), 1482–1487. ISSN: 0263-2241. DOI: https://doi.org/10.1016/j.measurement.2012.11.041. URL: https://www.sciencedirect.com/science/article/pii/S0263224112004629 8.

[ZLX*24] ZHANG, YUQING, LIU, YUAN, XIE, ZHIYU, et al. "DreamMat: High-quality PBR Material Generation with Geometry- and Light-aware Diffusion Models". *ACM Trans. Graph.* 43.4 (July 2024). ISSN: 0730-0301. DOI: 10.1145/3658170. URL: https://doi.org/10.1145/3658170 2.